Materials Science & Engineering A 578 (2013) 222–229

Contents lists available at SciVerse ScienceDirect

Materials Science & Engineering A

journal homepage: www.elsevier.com/locate/msea

Compression and low-velocity impact behavior of aluminum syntactic foam

G. Castro [a,*], S.R. Nutt [a], X. Wenchen [b]

[a] Department of Chemical Engineering and Materials Science, University of Southern California, Los Angeles, CA 90089-0241, USA
[b] School of Materials Science and Engineering, Harbin Institute of Technology, Harbin 15001, PR China

ARTICLE INFO

Article history:
Received 11 April 2013
Received in revised form
20 April 2013
Accepted 24 April 2013
Available online 2 May 2013

Keywords:
Aluminum foam
Ceramic microspheres
Compression
Low-velocity impact

ABSTRACT

We report quasi-static compression and impact behavior of aluminum syntactic foams (ASF) produced by melt infiltration. Aluminum syntactic foams with relative density of 0.46 were produced using hollow alumina spheres (4.45 mm and 3.05 mm) randomly situated in a mold and two types of aluminum alloy (1100 and 6061). The impact behavior was investigated using an instrumented drop tower. We investigated the influence of the matrix alloy, the size of ceramic spheres, and the addition of a face sheet on the quasi-static compression and impact behavior of ASF. The 1100 Al ASF absorbed greater energy at higher velocities (penetration) than the 6061 Al alloy ASF, although at lower impact velocities, both ASF's absorbed the same amount of energy (equal-energy interval). The use of smaller microspheres did not increase the amount of energy absorbed compared to ASF's with larger microspheres and comparable relative density. The use of face sheets significantly increased the energy absorption capacity of the ASF's. Failure mechanisms are interpreted from impact load–displacement curves and examination of the impacted ASF plates. The properties of the ASF were compared to conventional aluminum foam and steel syntactic foams. The compression strength and energy absorption of the ASF were greater than that of conventional Al foams, but less than that of steel syntactic foam produced using the same hollow alumina spheres.

1. Introduction

Metallic foams exhibit exceptional capacity to absorb energy when loaded in compression, much like conventional polymer foams, albeit with much greater strength, modulus, and heat resistance [1]. Potential applications include lightweight energy absorbing components for improving crashworthiness of motor vehicles, enhancing armor in military vehicles and structures, and blast-resistant structural panels. However most metallic foams to date are closed-cell "stochastic" structures characterized by inherent defects, including variations in cell wall thickness and non-uniform cell shapes and sizes. These defects lead to non-uniform, anisotropic material properties that are problematic when attempting to deploy the foams in structural applications [2]. These defects derive in part from the method of manufacture, which is a melt expansion process. Thus, realizing the potential of metallic foam as a structural material requires the elimination of defects by using a different method of production. Syntactic metal foams based on aluminum or Al alloys exhibit superior mechanical properties compared to stochastic foams, albeit at greater relative densities [3,4]. Syntactic foams are produced by infiltration of molten metal into an array of hollow ceramic spheres, resulting in a uniform pore size without the structural defects inherent in stochastic foams. The growing interest in metallic syntactic foams derives in large part from the substantially superior properties of Al-based syntactic foams relative to stochastic Al foams [5–8].

Although most reports on ASF have focused on the mechanical properties under static conditions [9], mechanical behavior under impact loading (high strain rates) is directly relevant to most of the intended applications. Test methods such as drop weight impact tests or split-Hopkinson pressure bars have been used to study the dynamic behavior of different types of ASF [5,7]. Impact testing reveals the resistance to high-rate loading and determines the energy absorbed in compression at high velocity. The objective of this work is to explore the dynamic impact behavior of ASF plates. We have studied the effect of the aluminum matrix alloy, size of microspheres, and the addition of a face sheet on the amount of energy absorbed during impact loading.

2. Experiment

2.1. Materials

Syntactic aluminum foams were produced from two primary constituent materials: aluminum (1100 and 6061 aluminum alloy) and hollow alumina spheres (Washington Mills Company). These

* Correspondence to: 15654 E. Grovecenter St., Covina, CA 91722, USA. Tel.: +1 626 388 7858; fax: +1 213 740 7797.
E-mail address: gerhardc@usc.edu (G. Castro).

0921-5093/$ - see front matter © 2013 Elsevier B.V. All rights reserved.
http://dx.doi.org/10.1016/j.msea.2013.04.081

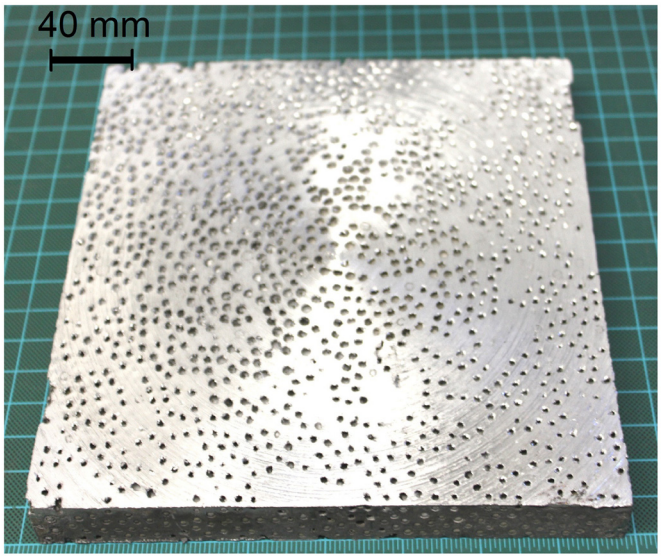

Fig. 1. Sample of aluminum syntactic foam produced by gravity-fed infiltration.

two alloys were selected to produce syntactic foams with different degrees of intrinsic strength and ductility. The spheres were sorted and classified according to size. Mono-sized alumina spheres with diameters of 4.45 ± 0.15 mm and 3.05 ± 0.14 mm were used for the infiltration experiments. These sizes were selected to minimize the resistance to melt infiltration. spheres less than 3 mm in diameter present greater resistance to melt infiltration [10]. The spheres were approximately spherical and showed a slight surface texture. In one sample variant, face sheets (Al 2024, 0.5 mm thick) were attached to the ASF plates. The face sheets were bonded to the ASF plates using a toughened epoxy film adhesive.

2.2. Foam production

A custom-designed stainless steel mold was used for the gravity-fed infiltration procedure. The mold consisted of an upper chamber for melting the aluminum charge, and a lower chamber for packing and infiltrating the alumina spheres. Aluminum charges were melted using a resistance furnace. After melting the aluminum charge in the upper chamber, the melt flowed through an opening in the bottom of the upper chamber, passed through a ceramic filter, and entered the mold, infiltrating the packed microspheres from bottom to top. Vents were machined in the mold to accommodate displaced gas during melt infiltration, avoiding air entrapment in the cast sample. This method also has been used to produce steel syntactic foam [4]. During the melt and infiltration process, the duration of each step was controlled to achieve reproducible and consistent samples, and experiments were carried out to determine the effects of process variables on foam quality.

Syntactic aluminum foams plates ($190 \times 190 \times 25.4$ mm^3) were prepared using the gravity-fed infiltration process shown in Fig. 1. The method yielded ASF with uniform distributions of spheres and negligible unintended porosity. The density of the syntactic foam was determined (by measuring weight and sample volume) to be 1242 kg/m^3, and the relative density of the ASF sample was 0.46 (aluminum density = 2700 kg/m^3).

2.3. Compression

Quasi-static compression tests were conducted at a strain rate of 1 mm/min using specimens with dimensions $24 \times 24 \times 24$ mm^3. Six samples for each type of ASF plate were prepared by polishing prior to testing. The samples were tested at room temperature in the as-cast condition. Compression tests were performed using a load frame (Instron 5567) and load–displacement data were converted to stress–strain data.

2.4. Impact

ASF plates were sectioned to final dimensions of $93 \times 93 \times 12.7$ mm^3 for impact testing. The samples were tested at room temperature and in the as-cast condition. Each impact test was performed on at least three replicates. The impact tests on the ASF plates were performed using an instrumented drop tower (DynaTup 9250HV). Fig. 2 shows the drop tower and a schematic view of the machine.

A hemispherical steel tup of 16.1 mm diameter was used as the indenter. The ASF plates were placed between top and bottom clamp plates, ensuring that the mid-point of the plate was positioned directly underneath the tup (central impact). The impact weight (6.4 kg) was released from a preset height and fell freely along two guide columns and through the center hole of the clamp plates (Fig. 2b). Upon impact, the contact forces were recorded using a transducer mounted on the impactor, and the force–time history was recorded in a computer. The corresponding force–displacement history of the impactor was calculated by integration of the force–time history. If the impactor was assumed to be rigid, the force–displacement history of the impactor can be considered as the force–displacement response of the ASF plate, and the impact energy absorbed is calculated using this curve. We tested ASF plates consisting of 1100 Al/4.45 mm diameter spheres, 1100 Al/3.05 mm diameter spheres, 6061 Al/4.45 mm diameter spheres, and 1100 Al/4.45 mm diameter spheres reinforced with a face sheet of 2024 Al. The absorbed energy factor (absorbed energy normalized by the impact energy) is a common parameter used to evaluate the performance of samples at different impact energies. Images of post-test specimens were also recorded.

3. Results and discussion

3.1. Quasi-static compression testing

The stress–strain curves of all tested ASF samples exhibit elastic–plastic stress–strain behavior characteristic of metallic foams and other cellular materials (Fig. 3). The first stage consists of a linear elastic region culminating in a distinct knee. The stress at this knee is taken as the compression strength for the syntactic foam. The knee is followed by a protracted plateau, during which the cell walls bend, buckle and collapse. Note that the slope in this region gradually increases as deformation progresses and is not perfectly flat (plastic), as in an ideal energy absorber. Normally, strain hardening in metallic stochastic foams is insignificant, but the strain hardening that occurs during compression of the ASF samples is more pronounced because of the substantial thickness of the cell walls and the more uniform structure of the ASF plate [4]. Finally, the plateau ends and the stress rises sharply, as the spheres are completely collapsed and the densification stage begins.

Fig. 3 shows that the compression strength (and energy absorption capacity) of ASF Al 1100 is less than that of ASF Al 6061 for 4.45 mm spheres. The precipitation strengthening mechanism in the 6061 aluminum alloy matrix is primarily responsible for this difference [11]. Fig. 3 also shows that the compression strength of 1100 Al ASF/4.45 mm cells is greater than 1100 Al ASF/ 3.05 mm cells.

The mechanical properties of ASF under quasi-static conditions are compared to conventional aluminum foam [12] and steel syntactic foams [4] in Fig. 4. The compression strength of the ASF is greater than that of conventional Al foams. Likewise, the energy absorption per unit volume of the ASF is greater than that of the

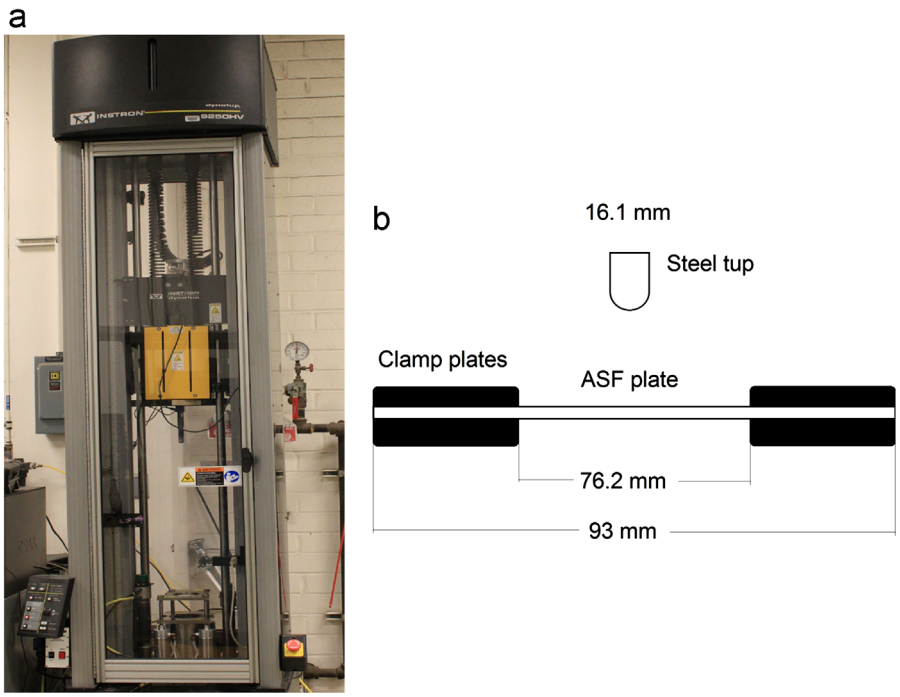

Fig. 2. (a) A picture and (b) schematic view of the drop tower testing machine.

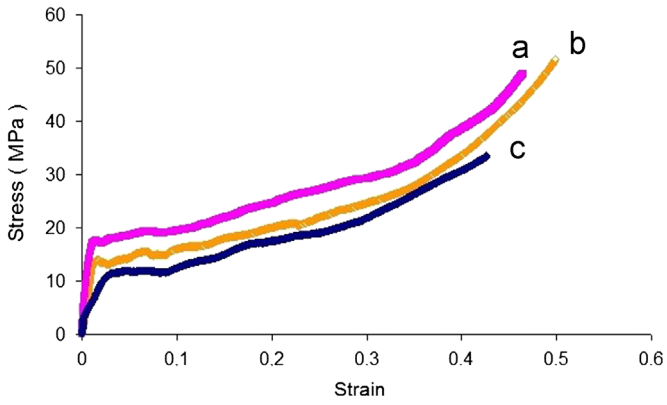

Fig. 3. Stress–strain curves for ASF. (a) Al 6061-4.45 mm sphere diameter. (b) Al 1100-4.45 mm sphere diameter. (c) Al 1100-3.05 mm sphere diameter.

conventional aluminum foams (14.55 MJ/m^3 versus 2.6 MJ/m^3), but less than that of steel syntactic foam (104.78 MJ/m^3), produced using the same type of hollow alumina spheres.

3.2. Impact behavior

Table 1 presents the results of all the different impact test done in the study, the values presented are average values. The effect of the aluminum alloy on the impact behavior of ASFs was analyzed by comparing ASF plates produced with different alloys and the same size spheres (4.45 mm). To present the results in context, we review the findings of Liu et al., who reported that the absorbed impact energy of composite laminates [13] was significantly low for impact energy values lower than the necessary for penetration threshold. As the impact energy increased, they found a range in which the absorbed energy was roughly equivalent to the impact energy (equal-energy interval), and two points bound this equal-energy interval. The lower bound was the penetration threshold, indicating the onset of penetration, while the upper bound was associated with perforation. As the impact energy increased beyond the perforation point, the amount of absorbed energy remained roughly constant (perforation zone) [13]. The absorbed energy factor decreases as the impact energy increases in the perforation zone.

Fig. 5 shows the force–displacement curves of the 1100 Al ASF tested with impact energies of 60, 120 and 180 J. When the ASF plates are subjected to impact energies of 60 and 120 J, partial penetration occurs. In this case, the force–displacement curves rise linearly, reach a maximum level and return to the origin, forming a closed loop that represents the impactor moving along with the ASF plate, stopping at the point of maximum displacement and then rebounding. The area enclosed by the closed curve is the energy that is absorbed by the ASF plate during the test. When the impact energy is increased to 180 J, complete perforation occurs and excess impact energy not absorbed by the sample is retained in the impactor as the indenter moves past the ASF plate. During impact at 180 J, the load first increases linearly with displacement up to an initial peak load. A plateau of ~12–14 mm displacement is observed after the initial peak load. A decrease in the load occurs when the sample is completely perforated. In this case, the force–displacement curve is no longer a closed loop, and the area bounded by the force–displacement curve and the displacement axis constitutes the energy absorbed by the perforated ASF plate.

For impact energies of 60 and 120 J, the absorbed energy factor is approximately 91%, indicating that the ASF plates absorb nearly all the impact energy in the form of damage, leaving only a small amount of energy for rebound (equal-energy interval). This behavior represents the behavior that an energy absorbing material is intended to exhibit. However, for an impact energy of 180 J, the absorbed energy factor drops to ~82%. The lower normalized absorbed energy indicates that the ASF samples are no longer able to absorb the entire impact energy at increasing impact velocities (perforation zone). Thus, the samples produced with 1100 aluminum alloy and 4.45 mm spheres exhibit perforation with a minimum absorbed energy of ~148 J.

Inspection of impacted samples in Fig. 6 revealed that the amount of damage increased with increasing impact energy, and damage is spread over an area larger than the area directly

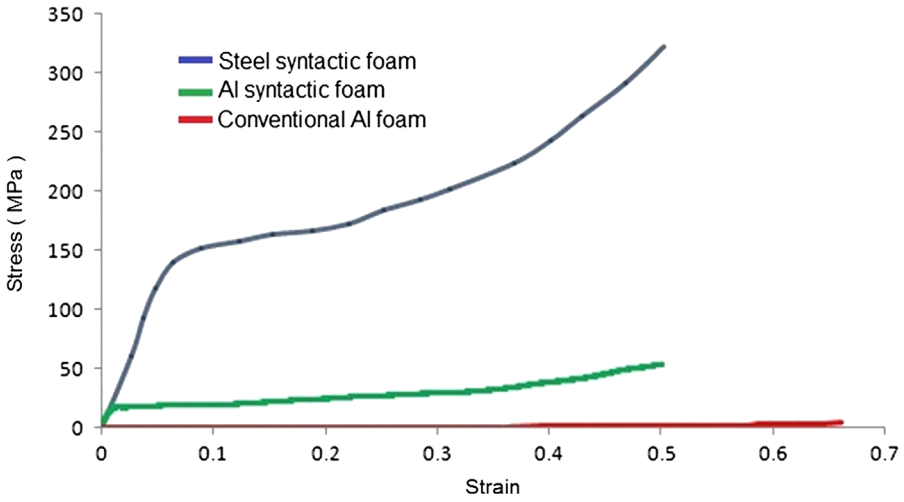

Fig. 4. Stress–strain curves for ASF(Al 6061-4.45 mm sphere diameter), SSF (4.45 mm sphere diameter) and conventional aluminum foam.

Table 1
ASF samples parameters, testing condition and impact results.

Aluminum matrix	Microsphere diameter (mm)	Impact energy (J)	Impact velocity (m/s)	Absorbed energy (J)	Absorbed energy factor	Perforation
6061	4.45	60	4.16	54.38	0.91	Partial
6061	4.45	120	5.92	111.46	0.93	Complete
6061	4.45	180	7.37	100.03	0.56	Complete
1100	4.45	60	4.18	54.26	0.90	Partial
1100	4.45	120	5.91	110.66	0.92	Partial
1100	4.45	180	7.30	148.41	0.82	Complete
1100+Al facesheet	4.45	60	4.19	53.13	0.89	Partial
1100+Al facesheet	4.45	120	5.92	111.66	0.93	Partial
1100+Al facesheet	4.45	180	7.38	175.47	0.97	Partial
1100	3.05	60	4.17	55.68	0.93	Partial
1100	3.05	120	5.94	92.95	0.77	Complete
1100	3.05	180	7.31	89.18	0.50	Complete

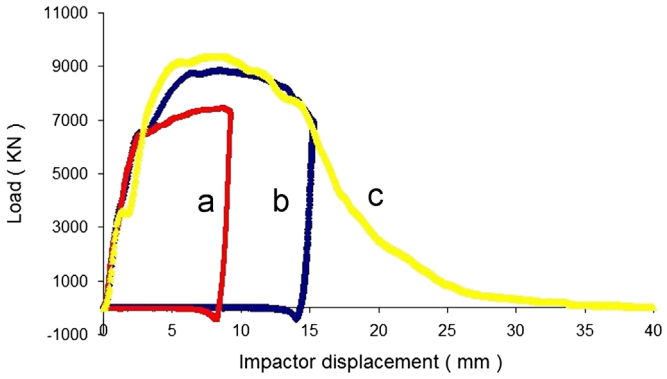

Fig. 5. Comparison of load–displacement behavior of ASF (1100 aluminum matrix-4.45 mm microsphere diameter) tested with different impact energies: (a) 60 J, (b) 120 J and (c) 180 J.

impacted by the indenter. The impact zone exhibited a ductile failure absent complete fracture or cracking of the ASF plates. For an impact energy of 60 J, radial cracks were observed at the back of the ASF plate. At impact energy of 120 J, larger cracks and a bulging formation were evident. At an impact energy of 180 J, the crack pattern produced a "petaling" failure and the indenter pushed off some pieces of foam. The resistance to impact of t he ASF plates is derived from collapsing and bending of the aluminum cell walls and crushing of the alumina spheres. Tearing of cell walls at the periphery of the impactor also contributed to the impact resistance [14]. Examination of the ASF "plugs" that resulted from complete penetration provided clear evidence for the failure mechanisms (collapsing, bending and tearing).

Fig. 7 shows the force–displacement curves of 6061 Al ASF tested with impact energies of 60, 120 and 180 J. An impact energy of 60 J produced partial penetration, while impact energies of 120 and 180 J produced perforation. For an impact energy of 60 J, the samples absorbed nearly all the impact energy—91% (equal-energy interval). For the 120 J impact energy, the ASF absorbed most of the impact energy while undergoing complete perforation. For 6061 Al ASF/4.45 mm spheres, a minimum absorbed energy of ~111.5 J was required to perforate the samples. Note that the force–displacement curve for the 180 J impact test exhibits features distinct from the other curves. First, there is a marked decrease in the maximum impact force, and this is reflected in the low absorbed energy. Second, there is a fracture event (brittle behavior) that is manifested as a fluctuation on the force–displacement curve (Fig. 7c). This indicates that the Al 6061 Al alloy fails in a brittle manner when the impact energy is 180 J.

Inspection of samples after impact revealed that damage was localized primarily in the area beneath the impactor (Fig. 8). There was also a small deformed area around the hole made by the impactor, although this was less pronounced in the case of ASF 1100 Al alloy plates. This type of failure can be described as ductile–brittle. At an impact energy of 60 J, small radial cracks were observed at the back of the ASF plate. At an impact energy of 120 J, the sample perforated and a "petaling" structure was evident at the back. At 180 J, complete perforation occurred, and the deformed foam was completely removed by the impactor (plugging). Damage in the 1100 Al alloy samples was spread over a larger area compared to the ASF 6061 Al alloy samples, which is

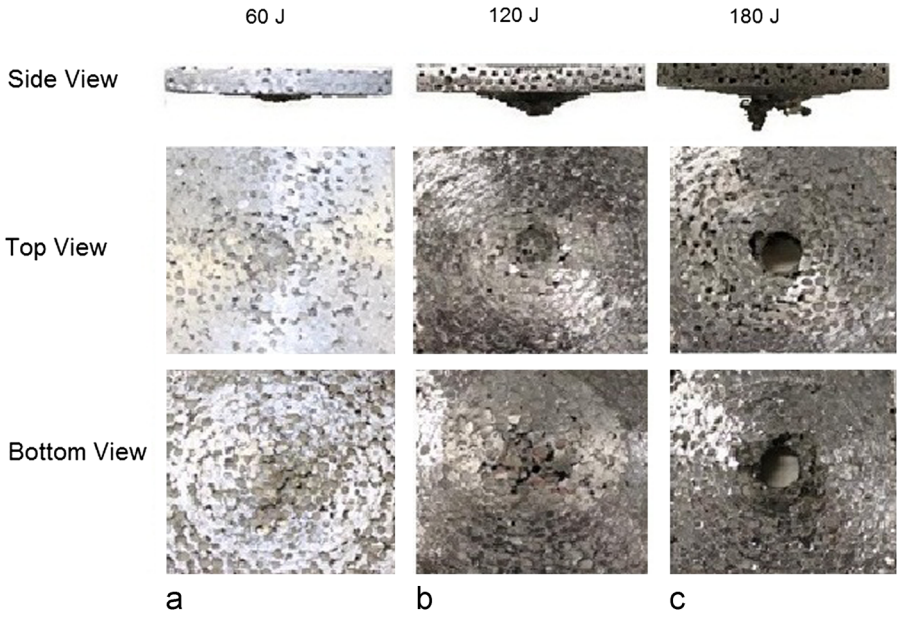

Fig. 6. Side, top and bottom views of the impacted specimens of ASF (1100 aluminum matrix-4.45 mm microsphere diameter) tested with different impact energies: (a) 60 J, (b) 120 J and (c) 180 J. Samples size is 93 mm × 93 mm × 12.7 mm.

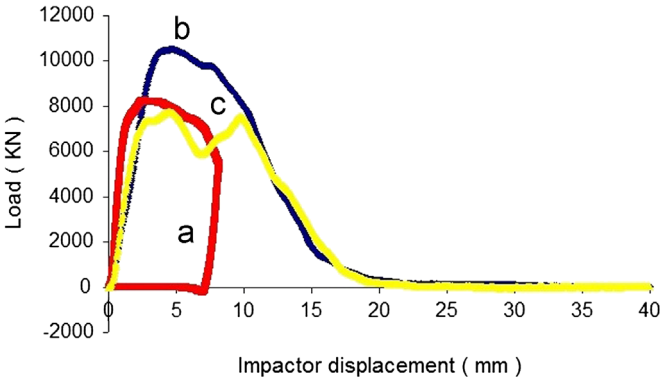

Fig. 7. Comparison of load–displacement behavior of ASF (6061 aluminum matrix-4.45 mm microsphere diameter) tested with different impact energies: (a) 60 J, (b) 120 J and (c) 180 J.

consistent with a greater energy absorbed. In essence, the 1100 ASF aluminum alloy absorbed a greater amount of energy before perforation than the 6061 alloy ASF. This differs from the ASF behavior under quasi-static loading conditions, where the 6061 Al ASF exhibited greater compression strength than the 1100 Al ASF.

3.3. Impact behavior of ASF with face sheet

The effect of adding a face sheet was analyzed by comparing the impact behavior of the 1100 Al ASF/4.45 mm cells with and without face sheets. Fig. 9 shows the load–displacement curves of 1100 Al ASF/4.45 mm cells with a 2024 alloy face sheet subjected to impact energies of 60, 120 and 180 J. None of the tested specimens were completely perforated, as shown in Fig. 10.

The absorbed energy factor is approximately the same for all the three impact energies (equal-energy interval). Adding the face sheet helps to increase minimum absorbed energy necessary for perforation. The addition of a face sheet increases the threshold perforation energy. Moreover, the final deflection is always less for the ASF sandwich plates than for the ASF cores alone. Similarly, the maximum impact force is always more for the ASF sandwich plates for the ASF cores alone. The observed increase in the threshold perforation energy for the sandwich plates is attributed to the bend/stretch resistance of the face sheet (Fig. 10). The use of face sheets is an effective means to increase the energy absorption capacity of the ASF plates while also increasing the resistance to bending loads. Alternative face sheet materials are contemplated for future studies [14].

3.4. Effect of cell size

The effect of the foam cell size was analyzed by comparing the impact behavior of the 1100 Al ASFs produced with 4.45 and 3.05 mm spheres. Fig. 11 shows the load–displacement curves of 1100 Al ASF (3.05 mm) tested with impact energies of 60, 120 and 180 J. Impact energies of 60 J produced partial penetration, while impact energies of 120 and 180 J caused perforation.

An impact energy of 60 J resulted in an absorbed energy factor of ~93% (equal-energy interval). The absorbed energy factors decreased as the impact energy increased (perforation zone), as shown in Table 1. ASFs produced with 1100 Al and 3.05 mm cells required a minimum absorbed energy of approximately 90 J to cause perforation. ASFs with larger cells (4.45 mm) exhibited greater perforation energy thresholds. Similarly, when loaded in compression at quasi-static rates, ASFs with larger cells exhibited larger strength values than those with smaller cells. Inspection of impacted samples revealed that the damage for the ASFs with different cell sizes was roughly similar—ductile failure occurred in both ASFs (Fig. 12).

There are conflicting reports in the literature on the relationship between cell size and compression strength in metallic syntactic foams. For example, Rohatgi reported decreasing compression strength with decreasing cenosphere size [15], and speculated that the greater void content in syntactic foams containing smaller size spheres might be responsible for the observed trend. Indeed, multiple studies report increasing compression strength with decreasing cell size [11,16,17]. In one report, ASF foams were produced with two different sizes of steel spheres (1.4 mm and 3.7 mm), and the ASF with the smaller cells showed greater compression strength [17]. In two studies, investigators reported that smaller spheres produced greater compressive strength values than larger spheres [11–16], speculating that

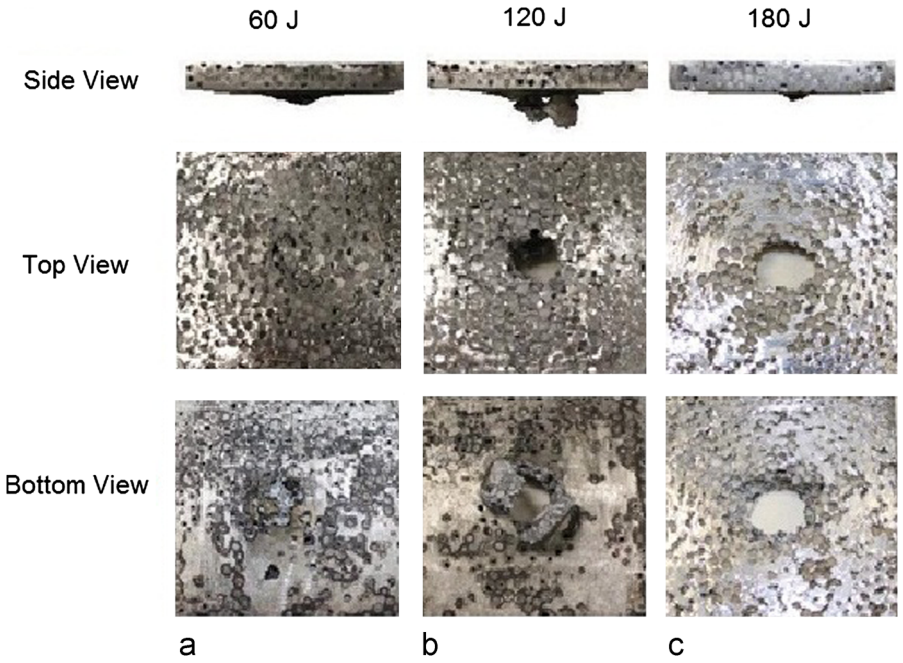

Fig. 8. Side, top and bottom views of the impacted specimens of ASF (6061 aluminum matrix-4.45 mm microsphere diameter) tested with different impact energies: (a) 60 J, (b) 120 J and (c) 180 J. Samples size is 93 mm × 93 mm × 12.7 mm.

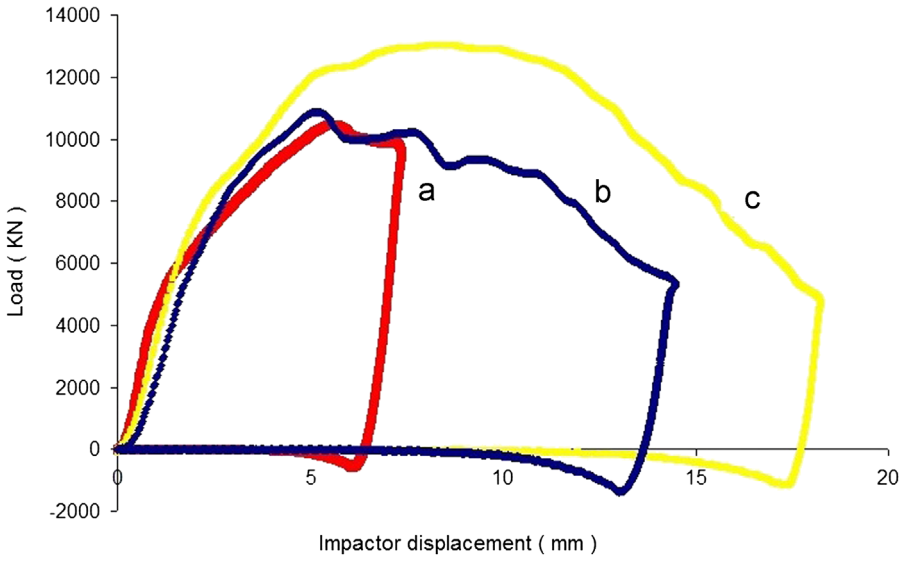

Fig. 9. Comparison of load–displacement behavior of ASF-1100 aluminum matrix-4.45 mm microsphere diameter+aluminum face sheet tested with different impact energies: (a) 60 J, (b) 120 J and (c) 180 J.

the greater curvature of smaller spheres imparted greater compressive strength and mechanical stability to the cells [11].

In addition to sphere size, the inherent strength of the spheres affects the strength of the resulting foam. Therefore, one must know the strength of the spheres to explain the compression strength of the resulting foams. Random groups of 30 spheres of each size (4.45 mm and 3.05 mm) were selected and compressed to failure [18]. Our results showed that the larger spheres were slightly stronger (31.85 N) than the smaller ones (28.78 N), which could explain in part why the larger spheres produced stronger foams. The lower strength of the smaller spheres could be related to sphere morphology, method of manufacture, and variability of wall thickness [19]. Further work will be required to better understand the effect of sphere size on the mechanical properties of the ASF plates. There have been suggestions on the literature advocating for the use of high quality engineered hollow spheres produced by powder metallurgy (instead of melt atomization), although such spheres are most costly than those used in the present study [7].

We now compare the performance of the aluminum syntactic foam produced in this study with the performance of aluminum "stochastic" foam under impact loading. Mohan et al. reported that closed cell Al foam with an average relative density of 9.5% and 20 mm thick exhibited an energy absorption factor of 21% when impacted with an impact energy of nearly 60 J. In this case, it is estimated that the impact energy threshold for perforation is ~12.6 J for the aluminum "stochastic" foam. Although ASF samples in the present study were tested at different conditions (samples

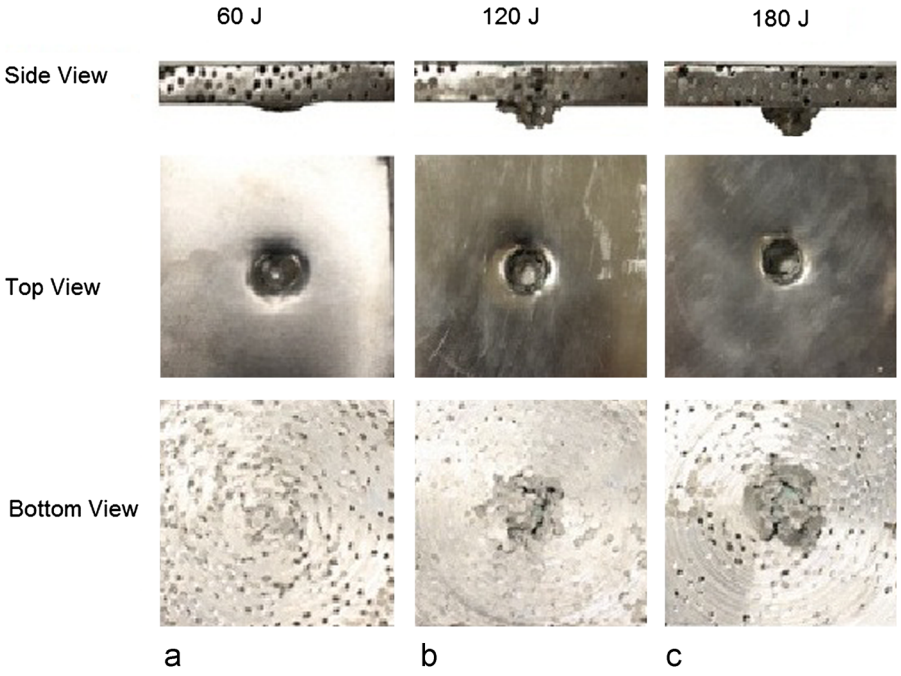

Fig. 10. Side, top and bottom views of the impacted specimens of ASF-1100 aluminum matrix-4.45 mm microsphere diameter+aluminum face sheet tested with different impact energies: (a) 60 J, (b) 120 J and (c) 180 J. Samples size is 93 mm × 93 mm × 12.7 mm.

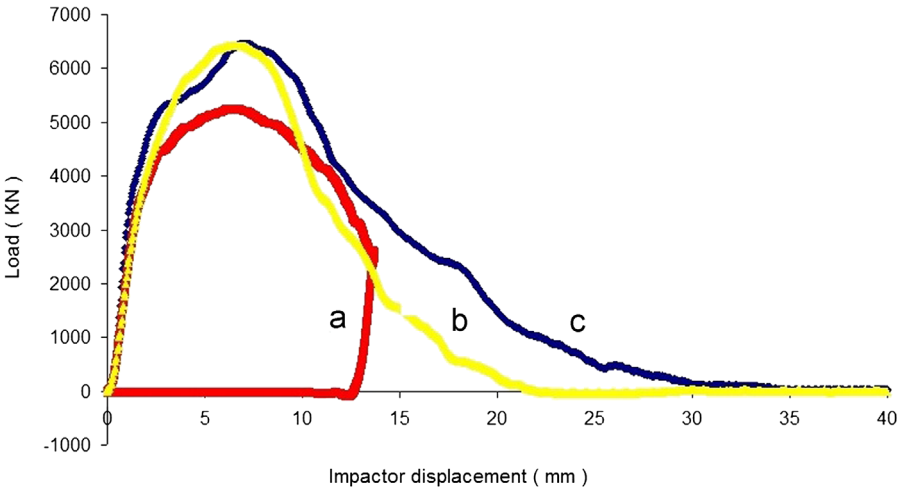

Fig. 11. Comparison of load–penetration depth behavior of ASF (1100 aluminum matrix-3.05 mm microsphere diameter) with different impact energies: (a) 60 J, (b) 120 J and (c) 180 J.

12.7 mm thick), the impact energy threshold for perforation is nearly twelve times greater than that of aluminum stochastic foam (148 J versus 12.6 J). Normalizing the impact energy threshold for perforation by volume and mass of the plate shows the advantage of the aluminum syntactic foam (1.35 MJ/m^3 and 1.08 kJ/kg) with respect to aluminum "stochastic" foam (0.063 MJ/m^3 and 0.25 kJ/kg).

4. Conclusions

The mechanical properties of ASF (static and dynamic) have been investigated. Under quasi-static conditions, ASF exhibits greater strength and energy absorption capacity than conventional aluminum foams, but lower than SSF. ASF (along with steel syntactic foams) are potentially useful in applications requiring high energy absorption. The mechanical properties of the syntactic metal foam can be tailored by choice of an appropriate metal matrix (either an aluminum or steel alloy) according to the required energy absorption and maximum stress allowable.

Low-velocity impact testing of ASF showed that 1100 Al (ductile) exhibited greater perforation resistance than the Al 6061 (hardened) under the impact speeds used in this study. Greater impact energy is required to achieve perforation in the Al 1100 alloy matrix (148.41 J compared to 111.5 J). The use of smaller spheres did not increase the amount of energy absorbed compared to ASF's with larger spheres and comparable relative density. The use of face sheets significantly increased the energy absorption capacity of the ASF's. Future effort will be devoted to optimizing the energy absorption properties of ASF under dynamic loading conditions.

Aluminum syntactic foams produced by melt infiltration are promising materials for energy absorption applications. Multiple approaches can be explored to improve mechanical properties,

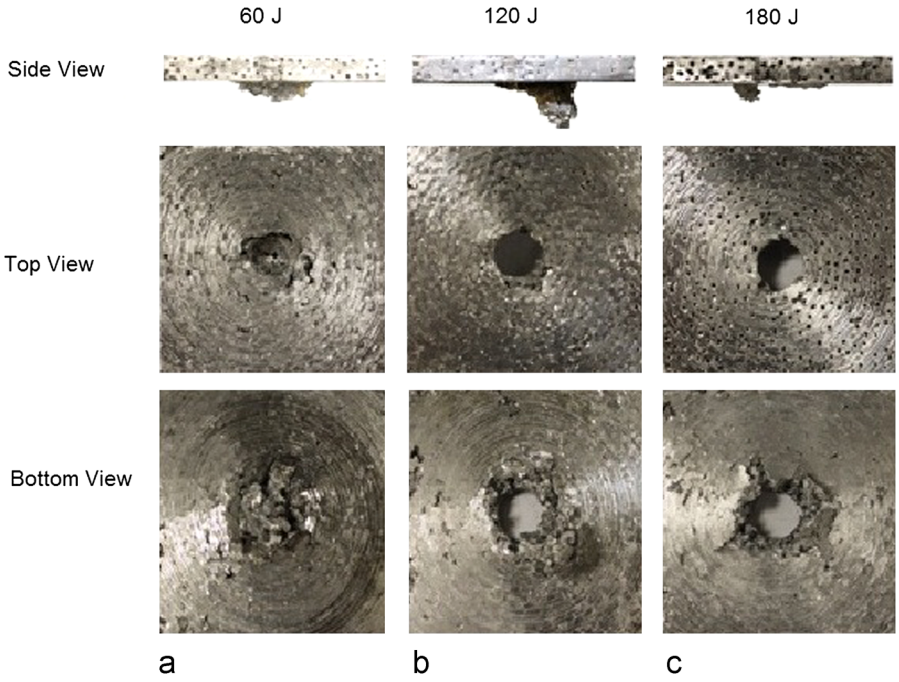

Fig. 12. Side, top and bottom views of the impacted specimens of ASF (1100 aluminum matrix-3.05 mm microsphere diameter) with different impact energies: (a) 60 J, (b) 120 J and (c) 180 J. Samples size is 93 mm × 93 mm × 12.7 mm.

including matrix reinforcement [5], addition of nanoparticles [20] and heat treatment after foam casting. The gravity-fed infiltration method can be extended to molds with different geometries and sizes, and is potentially an economical way to produce ASFs of different shapes, sizes, and cell size. Potential ASF applications include lightweight energy absorbing components for improving crashworthiness of motor vehicles, enhancing armor in military vehicles, and blast-resistant structures.

References

[1] J. Banhart, Mater. Adv. Eng. Mater. 8 (9) (2006) 781–794.
[2] M. Mukherjee, F. Garcia-Moreno, J. Banhart, Scr. Mater. 63 (2) (2010) 235–238.
[3] G. Castro, S.R. Nutt, Mater. Sci. Eng. A 535 (2012) 274–280.
[4] G. Castro, S.R. Nutt, Mater. Sci. Eng. A 553 (2012) 89–95.
[5] D.K. Balch, J.G. O'Dwyer, G.R. Davis, C.M. Cady, G.T. Gray III, D.C. Dunand, Mater. Sci. Eng. A391 (1–2) (2005) 408–417.
[6] L.C. Zou, Q. Zhang, B.J. Pang, G.H. Wu, L.T. Jiang, H. Su, Mater. Des. 45 (2013) 555–560.
[7] D.D. Luong, O.M. Strbik III, V.H. Hammond, N. Gupta, K. Cho, J. Alloys Compd. 550 (2013) 412–422.
[8] M. Yu, P. Zhu, Y. Ma, Mater. Des. 47 (2013) 80–89.
[9] I.N. Orbulov, Acta Polytech. Hung. 9 (2) (2012) 1–15.
[10] R.A. Palmer, K. Gao, T.M. Doan, L. Green, G. Cavallaro, Mater. Sci. Eng. A 464 (2007) 85–92.
[11] I.N. Orbulov, J. Ginsztler, Composites: Part A 43 (2012) 553–561.
[12] D. Ruan, G. Lu, F.L. Chen, E. Siores, Compos. Struct. 57 (1–4) (2002) 331–336.
[13] D. Liu, B.B. Raju, X. Danga, Int. J. Impact Eng. 24 (2000) 733–746.
[14] K. Mohan, T.H. Yipa, S. Idapalapatib, Z. Chena, Mater. Sci. Eng. A 529 (2011) 94–101.
[15] P.K. Rohatgi, J.K. Kim, N. Gupta, S. Alaraj, A. Daoud, Compos. Part A: Appl. Sci. Manuf. 37 (2006) 430–437.
[16] G.H. Wu, Z.Y. Dou, D.L. Sun, L.T. Jiang, B.S. Ding, B.F. He, Scr. Mater. 56 (2007) 221–224.
[17] A. Rabiei, L.J. Vendra, Mater. Lett. 63 (2009) 533–536.
[18] K. Yan, X. Xie, B. Li, J. Yuan, J. Zhang, Mater. Sci. Eng. A 528 (2011) 8671–8675.
[19] M. Koopman, G. Gouadec, K. Carlisle, K.K. Chawla, G. Gladysz, Scr. Mater. 50 (2004) 593–596.
[20] X. Li, Y. Yang, AFS Trans. 133 (02) (2007) 1–12.